Article

Fast Deflagration-to-Detonation Transition in Helical Tubes

Igor O. Shamshin [1] , **Viktor S. Aksenov** [1,2], **Maxim V. Kazachenko** [1], **Pavel A. Gusev** [1] **and Sergey M. Frolov** [1,2,*]

[1] Semenov Federal Research Center for Chemical Physics of the Russian Academy of Sciences (FRC), Moscow 119991, Russia; igor_shamshin@mail.ru (I.O.S.); v.aksenov@mail.ru (V.S.A.); maksx71997@gmail.com (M.V.K.); gusevpa@yandex.ru (P.A.G.)

[2] Institute of Laser and Plasma Technologies, National Nuclear Research University "MEPhI", Moscow 115409, Russia

* Correspondence: smfrol@chph.ras.ru

Abstract: When designing a new type of power plants operating on pulsed detonations of gaseous or liquid fuels, the concept of fast deflagration-to-detonation transition (FDDT) is used. According to the concept, a flame arising from a weak ignition source must accelerate so fast as to form an intense shock wave at a minimum distance from the ignition source so that the intensity of the shock wave is sufficient for fast shock-to-detonation transition by some additional arrangements. Hence, the FDDT concept implies the use of special means for flame acceleration and shock wave amplification. In this work, we study the FDDT using a pulsed detonation tube comprising a Shchelkin spiral and a helical tube section with ten coils as the means for flame acceleration and shock amplification (focusing), respectively. To attain the FDDT at the shortest distances for fuels of significantly different detonability, the diameter of the pulsed detonation tube is taken close to the limiting diameter of detonation propagation for air mixtures of regular hydrocarbon fuels (50 mm). Experiments are conducted with air mixtures of individual gaseous fuels (hydrogen, methane, propane, and ethylene) and binary fuel compositions (methane–hydrogen, propane–hydrogen, and ethylene–hydrogen) at normal pressure and temperature conditions. The use of a helical tube with ten coils is shown to considerably extend the fuel-lean concentration limits of detonation as compared to the straight tube and the tube with a helical section with two coils.

Keywords: pulsed detonation tube; fast deflagration-to-detonation transition; run-up distance; detonability; hydrogen; methane; propane; ethylene; blended hydrogenous fuels

1. Introduction

There are two known scenarios of deflagration-to-detonation transition (DDT) in tubes with gaseous explosive mixtures or gas suspensions of droplets and solid particles. In the first, classical DDT [1–3], the ignition of the mixture by a weak ignition source leads to the appearance of a flame, which, while propagating along the tube, changes its shape, increasing the combustion surface, and accelerates, forming compression and shock waves, eventually leading to the self-ignition of a shock-compressed explosive mixture and the onset of detonation. At the stage of flame acceleration, the most important role is played by gas-dynamic effects associated with the generation of turbulence ahead of the flame, for example, those produced with the help of the Shchelkin spiral [4–6] or regular orifice plates [7–9]. The second scenario was developed for the design of a new type of power plants operating on pulsed detonations and is referred to as fast DDT (FDDT) [10,11]. In this scenario, the flame arising from a weak ignition source must accelerate so fast as to form an intense shock wave at a minimum distance from the ignition source so that the intensity of the shock wave is sufficient for the fast shock-to-detonation transition caused by some additional arrangements in the detonation tube. Hence, the FDDT concept implies the use of special means for flame acceleration and shock wave amplification. Effective passive means of flame acceleration, in addition to the Shchelkin spiral and regular orifice

plates, include regular or irregular obstacles of a special shape [12–16] and snail-shaped channels with smooth walls [17]. The obstacles of a special shape provide the fastest flame acceleration with the minimal detrimental impact on the flame-born compression and shock waves traveling ahead of the flame. In snail-shaped channels, the flame propagation velocity increases exponentially rather than linearly, as in a straight channel, due to a large transverse velocity gradient. Fluidic obstacles generating intense turbulence for flame acceleration [18–20] and nanosecond repetitive pulsed plasma discharges [21–23] can be attributed to active means of flame acceleration.

Effective passive means of shock wave amplification include a single orifice plate [24], focusing nozzles [25,26] or central bodies [27] of special shapes, one or several U-turns of the detonation tube [28–32], annular channels [33,34], tube coils [35–38], etc. Active means of shock wave amplification include coherent energy deposition to a traveling shock wave triggered by an additional single electrical discharge or distributed electrical discharges [39–43] or by creating a cloud of chemically activated gas in the path of the shock wave [44,45]. Generally speaking, the use of the FDDT concept allows one to maximize the energy potential of fuel for the fastest possible detonation initiation without applying strong ignition sources. This is possible by a proper redistribution of the available energy deposition in space and time.

The use of the FDDT concept with various means of flame acceleration and shock wave amplification allows us to develop and test a standard pulsed detonation tube (SDT-1) for ranking gaseous and liquid fuels by their detonability in mixtures with air using the measured FDDT run-up distance and time [46–50] as the detonability criteria, as well as to study the detonability of binary methane–hydrogen [51,52], propane–hydrogen [53,54], and ethylene–hydrogen [55,56] fuels in mixtures with air. According to Shchelkin [4], the run-up distance of DDT (if it exists) is proportional to the tube diameter; the smaller the diameter, the shorter the DDT run-up distance. The minimum (limiting) value of the tube diameter for the detonation of stoichiometric mixtures of alkane and alkene hydrocarbons larger than propane and propylene is about 50 mm, whereas lighter hydrocarbons (except for methane) and hydrogen exhibit lower limiting tube diameter values. Therefore, to minimize the size of the detonation tube in the experimental setup intended for the various hydrocarbons, we choose this value (50 mm) to cover the whole range of the hydrocarbons, at least for the mixtures of stoichiometric composition. It appears that the stoichiometric methane-air mixture is marginally detonable in the tube of such a diameter. Based on the existing knowledge, one could expect the detonability limits in the tube of larger diameter to be somewhat wider. However, keeping in mind the strong (U-shaped) dependence of the limiting tube diameter on fuel concentration, one could expect the concentration limits, starting from a certain value of tube diameter, to be independent of it. Due to the use of (i) a detonation tube with a diameter close to the limiting diameter of detonation propagation for air mixtures of regular hydrocarbon fuels (50 mm), (ii) a Shchelkin spiral, which provides fast flame acceleration, and (iii) a helical tube section with two coils, which provides the gas-dynamic focusing of the flame-born shock wave, the SDT-1 facility allows the reliable registration of FDDT in air mixtures of gaseous and liquid fuels with significantly different detonability (from methane and aviation kerosene to hydrogen) at the shortest distances (less than 2 m) and for the shortest times (less than 15 ms).

The most Important element of the SDT-1 facility is a helical tube section with two coils. This element allows the fast transition of a flame-born shock wave to a detonation at the shortest distances even in fuel-air mixtures of low detonability. The removal of the helical tube section from the SDT-1 facility, other things being equal, results in the failure of DDT for fuel-air mixtures, which do not exhibit DDT in a straight tube with a Shchelkin spiral. Calculations in [38] showed that successive reflections of the flame-born shock wave from the compressive wall in the coils produce hot spots with elevated temperature and pressure. These hot spots promote the onset of detonation. It is worth noting that similar hot spots arise during DDT and develop detonation propagation in straight tubes with Shchelkin spirals [57] or orifice plates [58]. In these cases, the hot spots originate due to

reflections of the flame-born shock wave or a detonation wave from the upstream surfaces of the obstacles. However, contrary to a helical tube with smooth walls, straight tubes with obstacles exhibit a considerable hydrodynamic drag, which deteriorates the conditions for shock amplification [10].

The objectives of this work are to"test'the new version of the standard pulsed detonation tube (SDT-2), in which the helical tube section with two coils is replaced by a helical tube section with ten coils, and to study the effect of the number of coils on the FDDT in air mixtures of individual gaseous fuels (hydrogen, methane, propane, and ethylene) and binary fuel compositions (methane-hydrogen, propane-hydrogen, and ethylene-hydrogen) at normal pressure and temperature (NPT) conditions. These objectives and the obtained results are the novel and distinctive features of this study.

2. Materials and Methods

2.1. Pulsed Detonation Tubes

Figure 1 shows the schematics of SDT-1 (Figure 1a) and SDT-2 (Figure 1b) with the numbers of the measuring ports (shown in bold), the distances between the measuring ports along the axial line, and the overall dimensions of individual sections. Additionally, the total lengths of the tubes along the centerline and the overall size of the tubes are indicated. Table 1 presents information on the sensors: ionization probes (Ips) and pressure sensors (PSs) installed in the measuring ports.

(a)

(b)
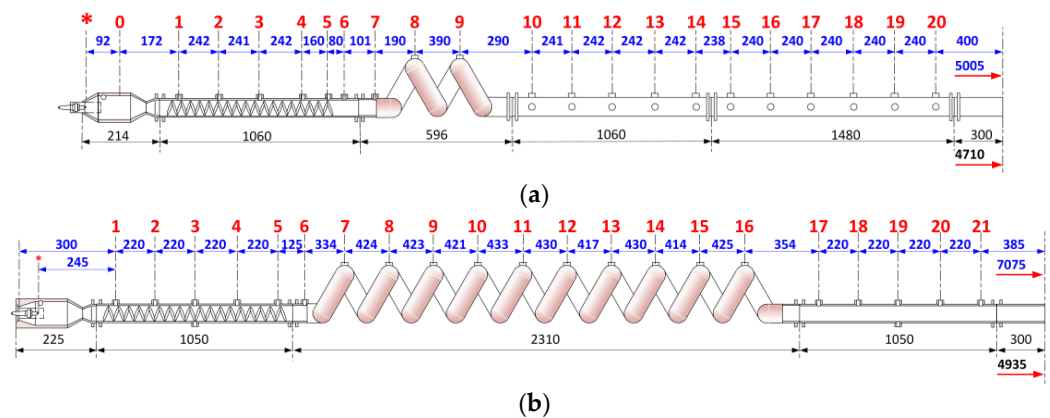
Figure 1. Schematics of SDT-1 (**a**) and SDT-2 (**b**). The asterisk shows the position of the spark gap.

Table 1. Schemes of installation of ionization probes (IP) and pressure sensors (PS) in SDT-1 and SDT-2.

Port#	0	1	2	3	4	5	6	7	8	9	10	11	12	13	14	15	16	17	18	19	20	21
											SDT-1											
IP	+	+	+	+	+	+	+	+	+	+	+	+	+	+	+	+	+	+	+	+	+	x
PS	x	−	−	−	+	+	+	+	+	+	+	+	+	+	+	+	−	−	−	−	−	x
											SDT-2											
IP	x	+	+	+	+	+	+	+	+	+	+	+	+	+	+	+	+	+	+	+	+	+
PS	x	−	−	−	+	+	+	+	+	+	+	−	+	−	+	−	+	−	−	+	−	+

Remarks: +, yes; −, no; x, no port.

The SDT-2 consists of the same structural elements as the SDT-1, namely, a prechamber with a spark plug (the position of the spark gap is shown by an asterisk in Figure 1), a flame acceleration section with a Shchelkin spiral, a helical tube section for the amplification of a flame-born shock wave, and a measuring section (a straight tube with smooth walls) for measuring the reaction wave (detonation) parameters after it exits from the helical tube section. Both tubes, SDT-2 and SDT-1, have an inner diameter of 50 mm. The geometric parameters of all structural elements of SDT-2 and SDT-1, except for the helical tube section

and the length of the measuring section, differ insignificantly. Thus, following the results of [51–56], the distance between the last turn of the Shchelkin spiral and the first coil of the helical tube in SDT-2 is reduced to 100 mm, whereas that of the SDT-1 is 150 mm. The Shchelkin spirals themselves are the same: they are wound from steel wire with a diameter of 6.7 mm; the spiral length is 940 mm; the outer diameter of the spiral is 49 mm; and the pitch of the turns is 24 mm. In contrast to that of SDT-1, the helical tube section in SDT-2 contains ten rather than two coils, whereas the average pitch of the coils is the same (216 mm). The measuring section in SDT-2 is approximately a factor of 2.5 shorter than that in SDT-1 (1000 mm vs. 2500 mm). Despite the fact that the length of the SDT-2 along the centerline is increased to 7075 mm (instead of 5005 mm for the SDT-1), the overall dimensions of the SDT-2 (4935 mm) and SDT-1 (4710 mm) are approximately the same. The internal volume of SDT-2 is increased by 4 dm^3: 14 dm^3 instead of 10 dm^3 for SDT-1.

2.2. Experimental Setup and Procedure

Figure 2 shows a schematic of the experimental setup with the SDT-2. The setup consists of a fuel-air mixture preparation and supply system, ignition system, control system, and data acquisition system. All systems are identical to those used in the experimental setup with SDT-1. The mixture is prepared in a 40 dm^3 mixer equipped with a fan. Before mixture preparation, the mixer is evacuated to a pressure of less than 0.1 kPa using a vacuum pump. The mixture is prepared by partial pressures. The pressure is determined with an accuracy of 0.1 kPa. Molecular mixing of the components is achieved by turning on the fan located inside the mixer for 20 min.
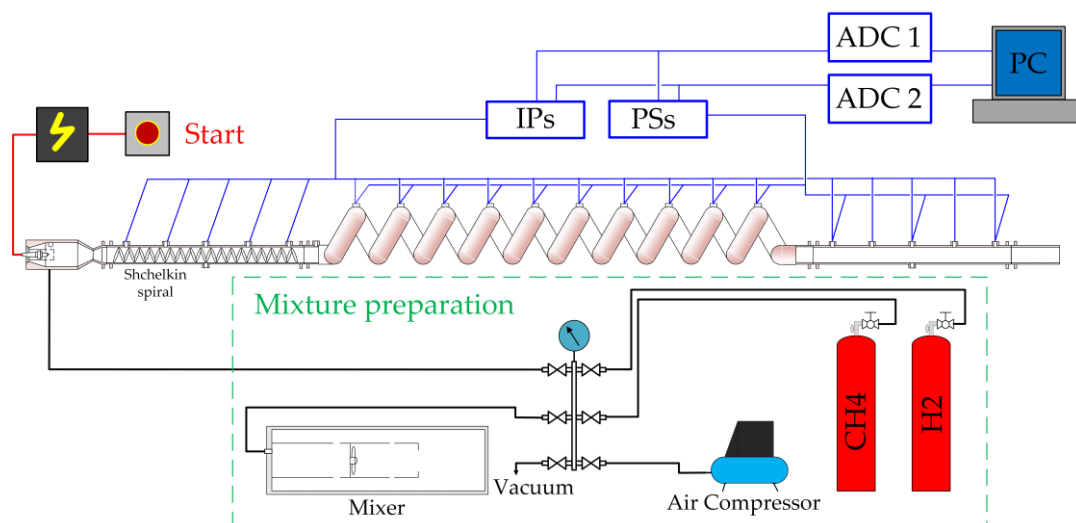
Figure 2. Schematic of the experimental setup with SDT-2.

The SDT-2 is filled with a fuel-air mixture in the following way. First, the tube is purged with compressed air. Thereafter, the tube is purged with the fuel-air mixture from the mixer until the volume of the purged mixture is four times the volume of SDT-2. The volume of the fuel-air mixture purged through the tube is controlled by the pressure drop in the mixer, whereas the flow rate of the mixture (10–20 L/min) is controlled by the vent valve. After the vent valve is closed, the ignition is triggered with a delay of 4 s. The number of experiments (hereinafter "shots") for fuel-air mixtures of a certain composition is normally 3. The instantaneous location and arrival time of the leading edge of the reaction front is determined using IPs [59]. The accuracy of determining the location and the arrival time of the reaction front using IPs is ± 2 mm and ± 1 μs. To record the pressure amplitude and profile in the shock and detonation waves, high-frequency piezoelectric PSs (PCB113B24) with a natural frequency of 500 kHz are used. The accuracy of determining the location of the pressure wave using PSs is ± 6 mm. From the IP and PS records, the

velocities of the reaction front and leading shock wave are calculated, respectively. The apparent velocity of the leading edge of the reaction front D_f on a measuring segment is determined by the known distance between the measuring ports with IPs along the axial line and by the time interval between the instants of arrival of the reaction front at these IPs. The propagation velocity of the flame-born pressure wave D_{SW} is determined similarly, but, instead of the IP records, the PS records are used. The error in determining the propagation velocity of the reaction front and pressure wave at $D_f > 1000$ m/s and $D_{SW} > 1000$ m/s is estimated at 3%. This allows one to build "time-distance" $(t - x)$ and "wave velocity-distance" $(D - x)$ diagrams of the development of the process. Joint consideration of the t–x and D–x diagrams allows one to determine the FDDT run-up distance L_{DDT} and time T_{DDT}. The values of L_{DDT} and T_{DDT} are the distance from the ignition source and the time from the ignition instant at which the reaction front velocity D_f reaches a steady-state value of the self-sustaining detonation velocity close to the thermodynamic Chapman-Jouguet (CJ) detonation velocity D_{CJ} for the fuel-air mixture under study. Self-sustaining detonation is understood as the steady-state reaction wave propagating at an average velocity, which is constant within $\pm$ 3%, whereas the fronts of the reaction and the leading shock wave merge within $\pm$ 6 µs. Particular attention is paid to the reproducibility of the results; a detonation wave is considered to be established if it propagates with approximately the same supersonic speed in all shots with the fuel-air mixture of a given composition. The errors in determining L_{DDT} and T_{DDT} are the maximum deviations of the values of L_{DDT} and T_{DDT} from the arithmetic mean in 3 successive shots. The minimum absolute error in determining L_{DDT} corresponds to half the length of the measuring segment on which the FDDT is registered. To refine the values of L_{DDT}, the trajectory of the detonation wave recorded with the help of PSs is used.

2.3. Gases

The pressurized gases used in the experiments are air, hydrogen, methane (natural gas), propane, and ethylene at $T_0 = 300$ K. The gases provided by the manufacturer are commercial-grade (99.9% purity) hydrogen, propane, and ethylene. The room air is compressed by an oil-free air compressor (Fubag OL195/6 CM1.5, Fubag GmbH, Germany) and used as an oxidizer. The composition of the natural gas is presented in Table 2. As can be seen, the volume fraction of methane in the natural gas is 94.8%.

Table 2. Natural gas composition (%vol.).

CH_4	C_2H_6	C_3H_8	i-C_4H_{10}	n-C_4H_{10}	C_5H_{12}[1]	C_6H_{14}[2]	C_xH_y[3]	N_2
94.8	2.8	0.84	0.12	0.14	0.05	0.02	0.03	1.2

[1] the sum of pentanes (isopentane, n-pentane, neopentane); [2] the sum of hexanes (n-hexane, 2,2-dimethylbutane, 2-methylpentane, and 3-methylpentane); [3] the sum of other hydrocarbons.

3. Results and Discussion

This section discusses the results of experiments on the FDDT in the SDT-2 facility in air mixtures of hydrogen, methane, propane, and ethylene, as well as in air mixtures of binary methane-hydrogen, propane-hydrogen, and ethylene-hydrogen fuels, under NPT conditions. Where possible, the experimental results are compared with those obtained in SDT-1.

3.1. Hydrogen-Air Mixtures

Experiments with hydrogen-air mixtures showed that the FDDT occurred in a very similar way in both SDT-1 and SDT-2 over a wide range of compositions determined by the value of the fuel-to-air equivalence ratio Φ. Figure 3 compares the dependences of the reaction front velocity D_f and shock wave velocity D_{SW} measured in SDT-1 (Figure 3a) and in SDT-2 (Figure 3b) on the axial distance from the ignition source x for a hydrogen-air mixture with $\Phi \approx 0.5$ (hydrogen volume fraction in the mixture $x_{H2} = 17.2$–17.3%(vol.)).

From now on, the vertical dash-dotted lines in the figures show the beginning and end of the helical tube section in SDT-1 and SDT-2, and the horizontal dashed line shows the CJ detonation velocity D_{CJ}. The yellow vertical bar corresponds to the experimental spread of the measured FDDT run-up distance L_{DDT}. In SDT-1, the FDDT in a mixture with $\Phi \approx 0.5$ occurred at the exit from the helical tube section at a distance L_{DDT} = 2.2–2.3 m with a steady-state value of the detonation velocity in the measuring section $D \approx 1585 \pm 15$ m/s. The CJ detonation velocity for this mixture was D_{CJ} = 1607 m/s. This means that the detonation propagated with the velocity deficit $\Delta D/D_{CJ} = (D_{CJ} - D)/D_{CJ} \approx 1\%$. In SDT-2, the FDDT occurred in a similar way between the second and third coils at a distance L_{DDT} = 2.2–2.5 m; however, the steady-state value of the detonation velocity in the helical tube section was noticeably lower ($D = 1490 \pm 20$ m/c) than the CJ detonation velocity, so that the detonation velocity deficit was $\Delta D/D_{CJ} \approx 7\%$. When the detonation wave entered the measuring section of SDT-2, the detonation velocity increased to $D = 1540 \pm 20$ m/s, and the detonation velocity deficit decreased to $\Delta D/D_{CJ} \approx 1\%$.
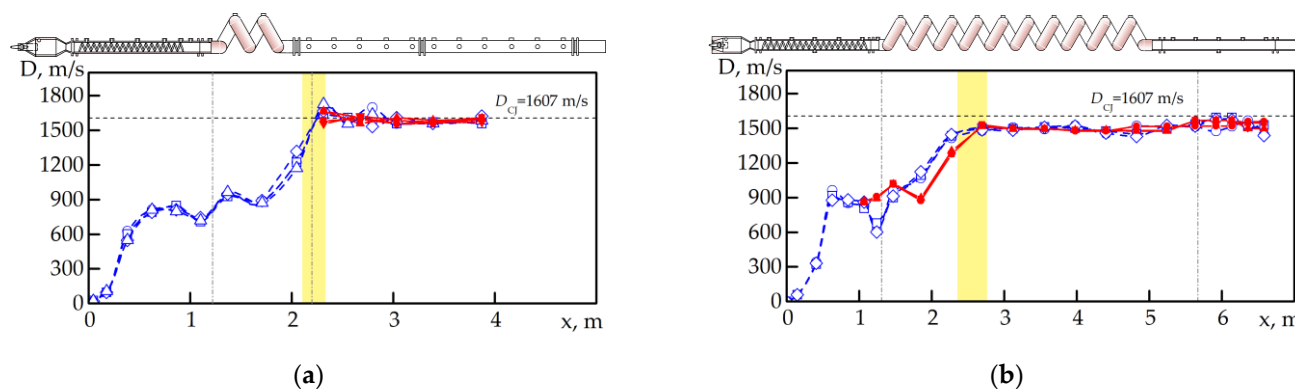
Figure 3. D–x diagrams for several shots with a fuel-lean hydrogen–air mixture with $\Phi \approx 0.5$: (**a**) 17.2%(vol.) H_2–air mixture, SDT-1; (**b**) 17.3%(vol.) H_2–air mixture, SDT-2. Horizontal dashed lines correspond to the CJ detonation velocity D_{CJ}; different symbols correspond to different shots; empty symbols connected by a dotted line correspond to the reaction front velocity D_f; filled symbols connected by a solid line correspond to the shock wave velocity D_{SW}.

When the hydrogen content in the hydrogen-air mixture decreased below $\Phi \approx 0.5$, the maximum velocity of the reaction front in the Shchelkin spiral decreased, and, at a certain limiting value, $\Phi = \Phi^*$, the FDDT failed to occur. The value of Φ^* in SDT-2 turned out to be lower than in SDT-1, which means that the fuel-lean concentration limit of FDDT in SDT-2 was extended. In confirmation of this, Figure 4 shows the dependences of the propagation velocities of the reaction front and flame-born shock wave on the distance measured in SDT-1 (Figure 4a) and SDT-2 (Figure 4b) for a hydrogen-air mixture with x_{H2} = 12%(vol.) ($\Phi^* \approx 0.325$). In SDT-1, there was no FDDT, while in SDT-2, the FDDT occurred in the seventh coil of the helical tube section at a distance $L_{DDT} \approx 4$ m, and the steady-state value of the detonation velocity in the helical tube section was $D = 1240 \pm 40$ m/s at D_{CJ} = 1385 m/s (velocity deficit $\Delta D/D_{CJ} \approx 10\%$). The extension of the fuel-lean concentration limit of FDDT in SDT-2 was obviously caused by the longer helical tube section and a larger number of successive reflections of the flame-born shock wave from the compressive wall in the coils, leading to a secondary explosion and detonation onset. The established detonation wave was capable of propagating in a smooth-walled helical tube with a large velocity deficit above 10%, which was apparently caused by the additional stabilizing effect of the transverse shock waves formed upon reflection of the detonation wave from curved surfaces. Previously [60], a similar velocity deficit (above 10%) was detected during the propagation of transient detonation waves in short tubes under the intense action of rarefaction waves. Interestingly, when entering the straight measuring section of SDT-2, the detonation wave decayed (see Figure 4b).

(**a**)　　　　　　　　　　　　　　　　　　　　(**b**)
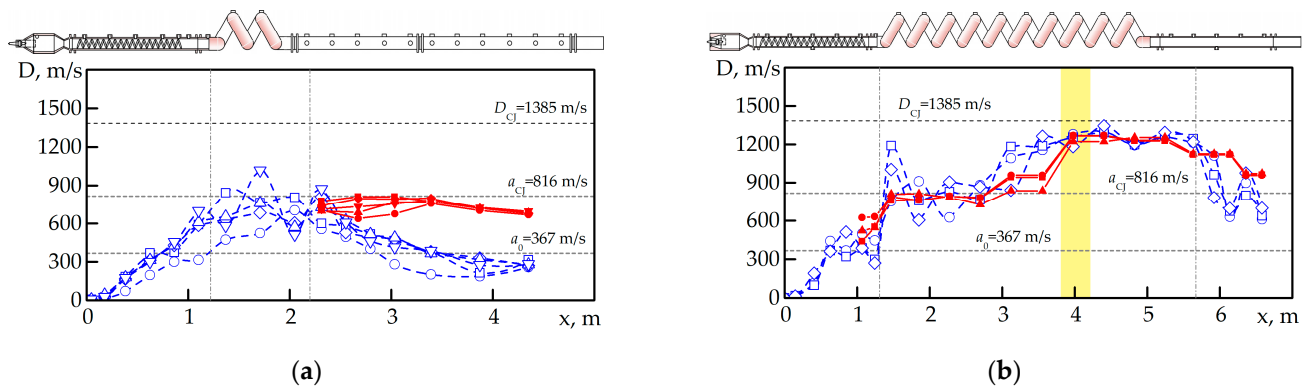
Figure 4. D–x diagrams for several shots with a fuel-lean 12%(vol.) H_2–air mixture ($\Phi \approx 0.325$): (**a**) SDT-1; (**b**) SDT-2. The horizontal dashed lines correspond (from bottom to top) to the speed of sound in the initial mixture, the speed of sound in the detonation products, and the CJ detonation velocity; different symbols correspond to different shots; open symbols connected by a dotted line correspond to the reaction front velocity D_f; filled symbols connected by a solid line correspond to the shock wave velocity D_{SW}.

Several important observations must be noted. First, the process evolution in the same segments of SDT-1 and SDT-2 facilities was about the same. This can be readily seen from Figures 3 and 4 for hydrogen-air mixtures with $\Phi \approx 0.5$ and 0.325. The evolution of the reaction front and shock wave velocities in the flame acceleration section and in the first two coils of the helical tube looked very similar. However, their further evolution looked different, apparently due to an additional effect of shock wave reflections from the curved surfaces in the longer helical tube of the SDT-2 facility. To demonstrate the effect of such reflections on DDT, let us consider Figure 5, which shows three successive snapshots of pressure isosurfaces in the course of shock wave propagation in a tube coil filled with a gaseous reactive mixture. These snapshots were obtained by calculations similar to those discussed in [38]. The incident shock wave propagates counterclockwise. As seen, shock wave propagation along the coil results in multiple reflections from the outer coil wall. One of the reflections at the 11 o'clock position results in the onset of detonation through the formation of a detonation "bubble" (see Figure 5a), its growth (see Figure 5b), and transformation to the overdriven detonation wave propagating in both directions, clockwise and counterclockwise (see Figure 5c).

(**a**)　　　　　　　　　　　(**b**)　　　　　　　　　　　(**c**)
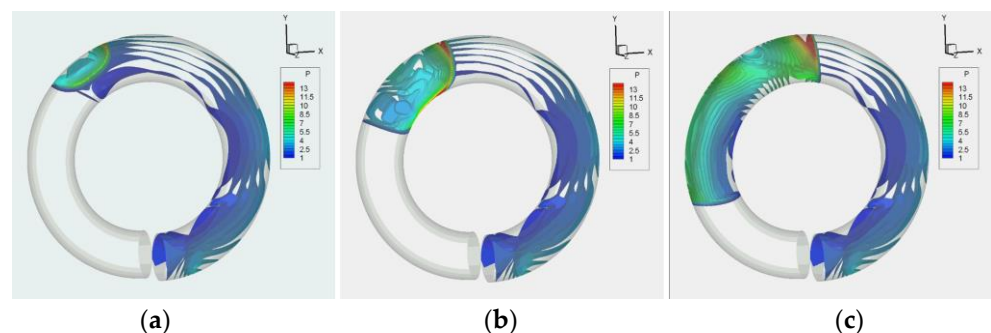
Figure 5. Three successive snapshots of pressure isosurfaces in the course of shock wave propagation (counterclockwise) in a tube coil filled with a gaseous reactive mixture; the pressure scale is in MPa. (**a**) Formation of a detonation bubble, (**b**) growth of the detonation bubble, and (**c**) propagation of the overdriven detonation in both directions.

Second, at the fuel-lean concentration limit of FDDT (at $\Phi = \Phi^*$), the minimum apparent propagation velocity of the reaction front at the inlet to the helical tube section was virtually constant and close to 400 m/s. As is shown later in this paper, for mixtures of hydrocarbon fuels with air, as well as for mixtures of binary hydrocarbon-hydrogen fuels, the minimum value of the apparent reaction front velocity at the fuel-lean concentration limit of FDDT (at $\Phi = \Phi^*$) was also almost constant and close to 500 m/s. Third, in SDT-1 and SDT-2, both the reaction front and the flame-born shock wave propagated at an almost constant velocity of about 800 m/s when entering the helical tube section. Fourth, in our previous experiments with spark ignition of the hydrogen-air mixture with $\Phi \approx 0.325$ at the closed end of a straight, smooth-walled tube with the same length-to-diameter ratio, the maximum measured propagation velocity of the reaction front reached only 40–80 m/s, and no tendency of the flame to accelerate was noted. In the experiments on SDT-1 and SDT-2, the apparent flame propagation velocity in the flame acceleration section (inside the Shchelkin spiral) increased to about 600 m/s and further increased to about 800 m/s in the helical tube section. Furthermore, in SDT-2, the FDDT led to the formation of the established detonation wave propagating steadily along the helical tube section. Thus, a sufficiently extended helical tube allows one to obtain the FDDT in fuel-air mixtures of extremely fuel-lean composition, such that classical DDT is impossible neither in straight tubes with smooth walls nor in straight tubes with rough walls.

Figure 6 shows the dependences of the propagation velocities of the reaction front and the flame-born shock wave measured in different sections of SDT-2 on the fuel-to-air equivalence ratio Φ in the hydrogen-air mixture. A decrease in hydrogen volume fraction from x_{H2} = 29.6%(vol.) (Φ=1) to x_{H2} = 15%(vol.) (Φ = 0.42) led to a decrease in the detonation velocity D in the measuring section of SDT-2 and to an increase in the detonation velocity deficit $\Delta D/D_{CJ}$ from approximately 1% to 6%. At x_{H2} < 15%(vol.), the detonation decayed in the measuring section of SDT-2, and the velocity of the flame-born shock wave decreased sharply from 1450 to 960 m/s when x_{H2} decreased from 15%(vol.) to 14%(vol.). Nevertheless, in the helical tube section, detonation propagated steadily at x_{H2} > 12%(vol.) (Φ = 0.325) with a velocity deficit $\Delta D/D_{CJ} \approx 10\%$, which was two times higher than the detonation velocity deficit for the detonation wave propagating in the fuel-air mixture of near-stoichiometric composition ($\Delta D/D_{CJ} \approx 5$–6%). Interestingly, when the hydrogen volume fraction in the mixture approached x_{H2} = 15%(vol.) (Φ = 0.42), the probability of detonation failure increased in the shots with the same mixture. Thus, at x_{H2} = 15.6%(vol.) (Φ = 0.44), detonation failed in one of three shots. The closer the mixture composition was to Φ = 0.42, the more shots with detonation failure were registered (see Appendix A). Transition from the steadily propagating detonation to a galloping mode (the mode with significant fluctuations in the detonation velocity) always occurred through a single-headed spin [61]. The domain of the galloping mode at the fuel-lean limit for hydrogen-air mixtures found in [61] corresponded to x_{H2} = 12.5–14.3%(vol.) or Φ = 0.34–0.40. In our study, this domain approximately corresponded to the domain x_{H2} = 12–15%(vol.) (Φ = 0.325–0.42), in which we registered detonation decay in the course of detonation transition from the helical tube section to the straight measuring section with smooth walls.

Figure 7 compares the measured detonation velocities in the measuring sections of SDT-1 and SDT-2 as a function of the fuel-to-air equivalence ratio Φ in fuel-lean and near-stoichiometric hydrogen-air mixtures. In SDT-1 and SDT-2, the FDDT was registered at Φ > 0.48 and Φ > 0.32, respectively. According to the literature data, when the detonation is obtained by direct initiation, the lower concentration limit of detonation propagation in tubes of different diameter d filled with the hydrogen-air mixture is x_{H2} = 18.3%(vol.) (Φ = 0.53 [62]) and x_{H2} = 12.5%(vol.) (Φ = 0.34, d up to 30 cm [61]). The use of a combination of Shchelkin spiral and a helical tube section with ten coils allowed approaching the lower concentration limit of detonation reported in [61] via FDDT rather than via direct detonation initiation.
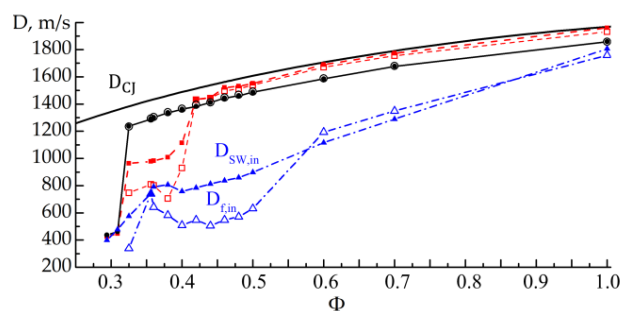
Figure 6. Dependences of the propagation velocities of the reaction front and the flame-born shock wave measured in different sections of SDT-2 on the fuel-to-air equivalence ratio Φ in the hydrogen–air mixture. The solid curve corresponds to the CJ detonation velocity D_{CJ}; open symbols correspond to the reaction front velocity D_f; filled symbols correspond to the shock wave velocity D_{SW}; squares connected with a dashed line correspond to the velocities in the measuring section; circles connected with a solid line correspond to the velocities measured in the helical tube section; triangles connected with a dash-dotted line correspond to the velocities at the inlet to the helical tube section.

Figure 7. Comparison of the measured detonation velocities in the last coil of the helical tube section in SDT-1 and SDT-2 with fuel-to-air equivalence ratio Φ in the hydrogen–air mixture. The solid curve corresponds to the CJ detonation velocity D_{CJ}; open symbols correspond to the reaction front velocity D_f; filled symbols correspond to the shock wave velocity D_{SW}; squares connected with a dash-dotted line correspond to the velocities at the exit from the last coil of the helical tube section in SDT-1; circles connected with a dashed line correspond to the steady-state detonation velocities in the helical tube section in SDT-2.

The maximum measured DDT run-up distance for hydrogen-air mixtures was attained at $\Phi = 0.326$ (see Appendix A) with a value of 3.97 m along the facility centerline, i.e., DDT always occurred far from the end of the helical tube in the SDT-2 facility.

3.2. Methane-Air Mixtures

Experiments with methane-air mixtures were conducted at $\Phi = 0.7$, 0.8, 0.9, and 1.0 (see Appendix A). Figure 8 compares the dependences of the reaction front velocity D_f and the flame-born shock wave velocity D_{SW} measured in SDT-1 (Figure 8a) and SDT-2 (Figure 8b) on the distance for the methane-air mixture with $\Phi = 1.0$ (methane volume fraction $x_{CH4} = 9.5\%$(vol.)). The reproducibility of experiments in SDT-2 was seen to be much better than in SDT-1. However, when switching from a mixture with $\Phi = 1.0$ to a mixture with $\Phi = 0.9$, detonation decayed in the measuring section of SDT-2 in two of three shots, and, when switching to a mixture with $\Phi = 0.8$, it decayed in each shot. At $\Phi = 0.7$, at the exit from the Shchelkin spiral, the maximum apparent propagation velocity of the reaction front reached only 150 m/s, and the flame no longer accelerated in the helical tube section.

(a)

(b)
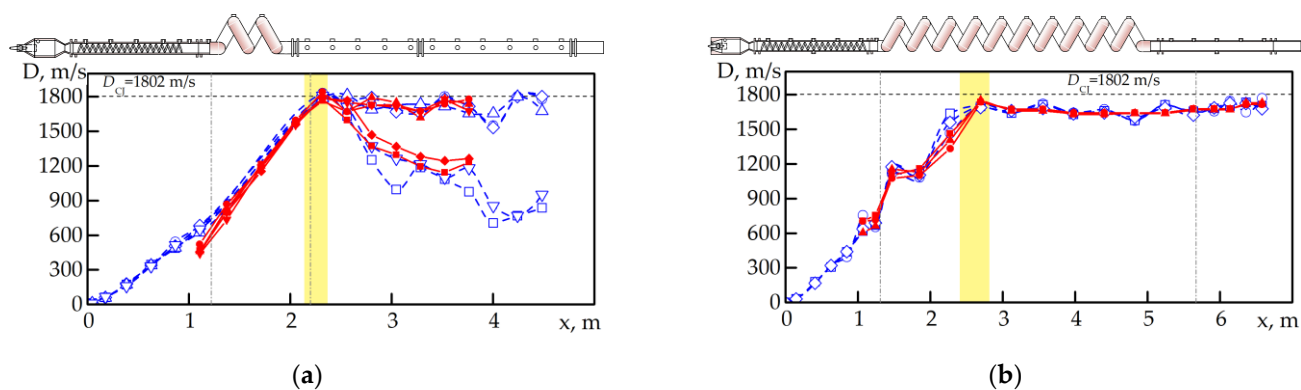
Figure 8. $D–x$ diagrams for several shots with the stoichiometric methane–air mixture ($\Phi = 1$): (**a**) SDT-1; (**b**) SDT-2. Horizontal dashed lines correspond to the CJ detonation velocity D_{CJ}; different symbols correspond to different shots; empty symbols connected by a dotted line correspond to the reaction front velocity D_f; filled symbols connected by a solid line correspond to the shock wave velocity D_{SW}.

The maximum measured DDT run-up distance for methane-air mixtures was attained at $\Phi = 0.8$ (see Appendix A) with a value of 4.04 m along the facility centerline, i.e., DDT always occurred inside the helical tube in the SDT-2 facility.

3.3. Methane-Hydrogen-Air Mixtures

The addition of methane to hydrogen led to the narrowing of the fuel-lean concentration limits of FDDT in SDT-2. Figure 9 shows an example illustrating this fact. The dilution of hydrogen with methane by 10%(vol.) (the fuel consisted of 10%(vol.) CH_4 and 90%(vol.) H_2) led to a shift in the lower concentration limit of FDDT from $\Phi = 0.32$ for a hydrogen-air mixture to $\Phi = 0.40$ for a 1% CH_4 + 10% H_2 + 89% air mixture. It can be seen from Figure 9 that at $\Phi = 0.38$ there was still no FDDT, and at $\Phi = 0.40$, FDDT occurred in the helical tube section with subsequent detonation decay when it entered the straight measuring section with smooth walls.

(a)

(b)
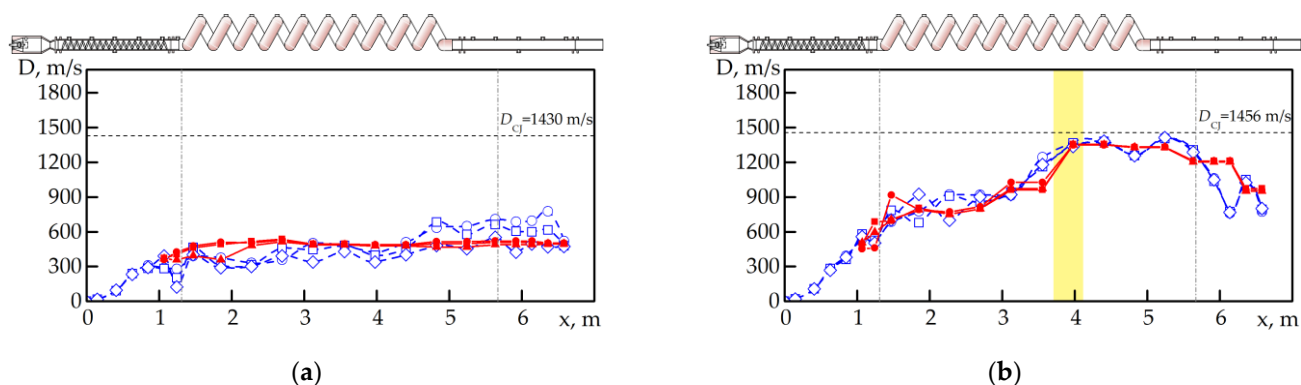
Figure 9. $D–x$ diagrams for several shots with the fuel-lean methane–hydrogen–air mixtures in SDT-2: (**a**) 1% CH_4 + 10% H_2 + 89% air mixture, $\Phi = 0.38$; (**b**) 1.14% CH_4 + 10.3% H_2 + 88.6% air, $\Phi = 0.40$. Horizontal dashed lines correspond to the CJ detonation velocity D_{CJ}; different symbols correspond to different shots; empty symbols connected by a dotted line correspond to the reaction front velocity D_f; filled symbols connected by a solid line correspond to the shock wave velocity D_{SW}.

Figure 10 shows the dependences of the propagation velocities of the reaction front and the flame-born shock wave measured in different sections of SDT-2 on the fuel-to-air equivalence ratio Φ in the blended methane-hydrogen (10% CH_4 + 90% H_2) fuel-air mixture. Similar to in hydrogen-air mixtures, there existed a range of compositions of

methane-hydrogen-air mixtures in which FDDT occurred in the helical tube section, and the arising detonation wave propagated steadily in this section but decayed when entering the straight measuring section with smooth walls.
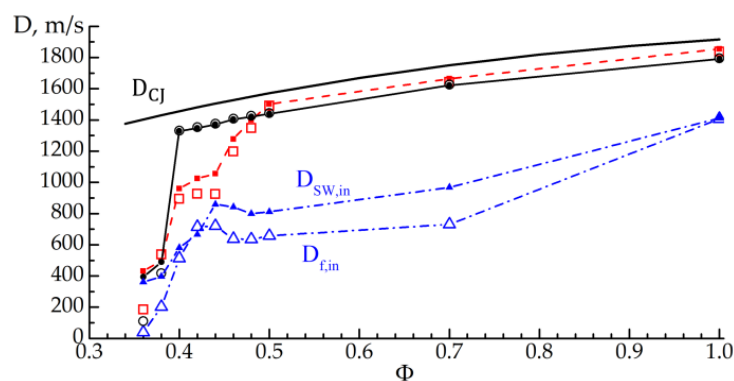
Figure 10. Dependences of the propagation velocities of the reaction front and the flame-born shock wave measured in different sections of SDT-2 on the fuel-to-air equivalence ratio Φ in the blended (10% CH_4 + 90% H_2) fuel–air mixture. The solid curve corresponds to the CJ detonation velocity D_{CJ}; open symbols correspond to the reaction front velocity D_f; filled symbols correspond to the shock wave velocity D_{SW}; squares connected with a dashed line correspond to the velocities in the measuring section; circles connected with a solid line correspond to the velocities measured in the helical tube section; triangles connected with a dash-dotted line correspond to the velocities at the inlet to the helical tube section.

Figure 11 shows the results of measurements of the detonation velocity in the helical tube section of SDT-2 for methane-hydrogen-air mixtures with different dilutions of hydrogen with methane. The modes of steady-state detonation propagation in the helical tube section followed by detonation decay in the measuring section (D/F modes) are marked with diamonds. With an increase in the methane content and a decrease in the hydrogen content in the fuel, the domain of existence of such D/F modes in terms of Φ shrunk, while the transition region itself was quite narrow. At the fuel-lean concentration limit of FDDT, the minimum apparent propagation velocity of the reaction front at the inlet to the helical tube section was almost constant and close to 500 m/s; when hydrogen was diluted with methane by 10, 20, 30, 40, and 50%, this velocity was 510 ± 10 ($\Phi^* \approx 0.40$), 500 ± 30 ($\Phi^* \approx 0.46$), 420 ± 80 ($\Phi^* \approx 0.50$), 520 ± 20 ($\Phi^* \approx 0.56$), and 500 ± 10 ($\Phi^* \approx 0.60$) m/s, respectively (see Appendix A).

According to the records of pressure sensors in the measuring section of SDT-2, detonation in methane-hydrogen-air mixtures near the fuel-lean concentration limit propagated in the spinning mode. Figure 12 shows an example of pressure records taken by three PSs in the measuring section of SDT-2 in three successive shots with the (20% CH_4 + 80% H_2)-air mixture at $\Phi = 0.54$. As seen, the detonation decayed in the first shot and propagated steadily in the spinning mode in the second and third shots. The spinning mode of detonation can be recognized from the pressure records. When the spinning detonation wave traveled along the tube and the spin head passed over the surface of a PS, the pressure record showed a sharp pressure rise or pressure peak on the background of a weaker shock wave. Similar pressure records were obtained for the (40% CH_4 + 60% H_2)-air mixture at $\Phi = 0.56$ (see D/F modes in Appendix A).

The maximum measured DDT run-up distance was attained for (30% CH_4 + 70% H_2)-air mixture at $\Phi = 0.5$ (see Appendix A) with a value of 5.61 m along the facility centerline, i.e., DDT always occurred inside the helical tube in SDT-2 or at the exit of the tenth coil.
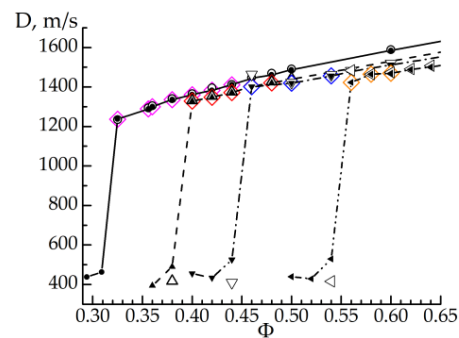
Figure 11. Dependences of the propagation velocities of the reaction front and the flame-born shock wave measured in the last coil of the helical tube section in SDT-2 on the fuel-to-air equivalence ratio Φ in methane–hydrogen–air mixtures with different dilution of hydrogen with methane. Open circles correspond to the reaction front velocity D_f; filled circles correspond to the shock wave velocity D_{SW}; circles connected with a solid line correspond to 100% H_2; triangles 8 and ▲ connected with a dashed line correspond to 10% CH_4 + 90% H_2; triangles X and ▼ connected with a dash-dotted line correspond to 20% CH_4 + 80% H_2; triangles Ξ and ◄ connected with a dash-double dotted line correspond to 40% CH_4 + 60% H_2; diamonds correspond to modes with steady detonation propagation in the helical tube section and detonation decay in the measuring section.
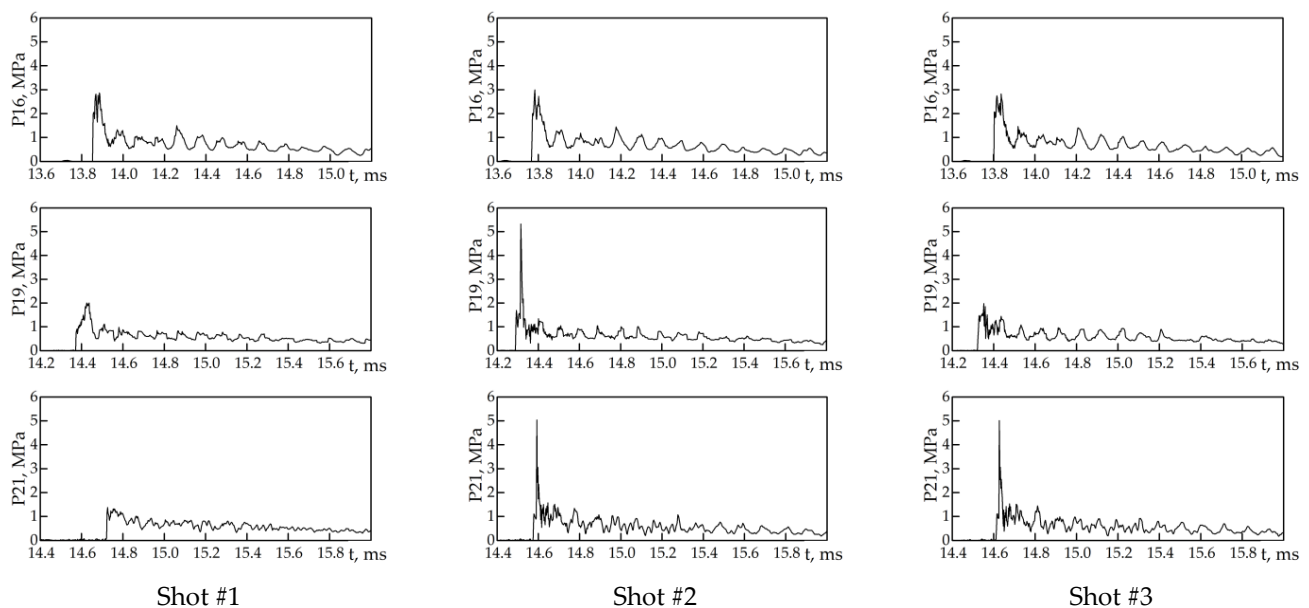
Figure 12. Records of pressure sensors 16, 19, and 21 in the measuring section of SDT-2 in three successive shots with (20% CH_4 + 80% H_2)–air mixture at $\Phi = 0.54$.

3.4. Propane-Hydrogen-Air Mixtures

When hydrogen was diluted with propane, the results obtained in SDT-2 were generally the same as those previously obtained in SDT-1 [33,34]. Figure 13 shows the dependences of the measured propagation velocities of the reaction front and flame-born shock wave in the measuring section of SDT-2 on the fuel-to-air equivalence ratio Φ of propane-hydrogen-air mixtures with different dilutions of hydrogen with propane (0, 10, 20, and 40%). At the fuel-lean concentration limit of FDDT, the minimum apparent propagation velocity of the reaction front at the entrance to the helical tube section was virtually constant and close to 500 m/s. When hydrogen was diluted with propane by 10% ($\Phi^* \approx 0.46$), 20% ($\Phi^* \approx 0.53$), and 40% ($\Phi^* \approx 0.62$), this velocity was equal to 510 ± 30, 400 ± 50, and 480 ± 60 m/s, respectively. Note that FDDT in a propane-air mixture (without hydrogen) occurs only at $\Phi \geq 0.72$ ($x_{C3H8} \geq 2.9\%$(vol.)), and there is no FDDT in the

leaner mixtures. In the propane-air mixture, the lower concentration limit of FDDT in SDT-2 (2.9%(vol.) C_3H_8) turned out to be slightly narrower than the lower detonability limits reported in [61] and [60] (2.3%(vol.) C_3H_8 and 2.6%(vol.) C_3H_8) for tubes 160 and 70 mm in diameter, respectively, but slightly wider than the limit of detonation reinitiation after it transitioned from a rough tube (a tube with a Shchelkin spiral) to a smooth-walled tube (3.5%(vol.) C_3H_8 [61]).
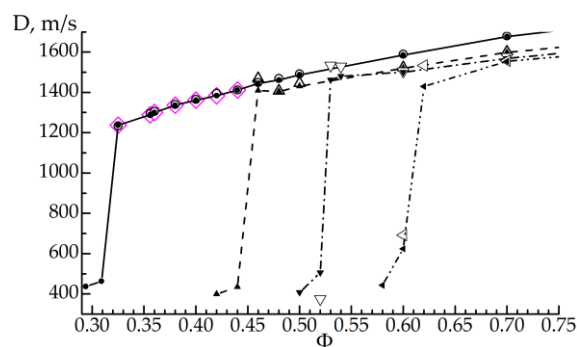
Figure 13. Dependences of the propagation velocities of the reaction front and the flame-born shock wave measured in the last coil of the helical tube section in SDT-2 on the fuel-to-air equivalence ratio Φ in propane–hydrogen–air mixtures with different dilutions of hydrogen with propane. Open circles correspond to the reaction front velocity D_f; filled circles correspond to the shock wave velocity D_{SW}; circles connected with a solid line correspond to 100% H_2; triangles 8 and ▲ connected with a dotted line correspond to 10% C_3H_8 + 90% H_2; triangles X and ▼ connected with a dash-dotted line correspond to 20% C_3H_8 + 80% H_2; triangles Ξ and ◄ connected with a double dash-dotted line correspond to 40% C_3H_8 + 60% H_2.

The maximum measured DDT run-up distance for propane-air mixtures was attained at $\Phi = 0.71$ (see Appendix A) with a value of 5.8 m along the facility centerline, i.e., DDT always occurred inside or shortly outside the helical tube of the SDT-2.

3.5. Ethylene-Hydrogen-Air Mixtures

Figure 14 shows the dependences of the propagation velocities of the reaction front and the flame-born shock wave in the measuring section of SDT-2 on the fuel-to-air equivalence ratio Φ of ethylene-hydrogen-air mixtures with dilutions of hydrogen with ethylene by 0, 10, 20, 30, and 40%. With a decrease in the hydrogen content in the fuel, the fuel-lean concentration limit of FDDT shifted to higher values of Φ from 0.32 (100% H_2) to 0.50 (60% H_2). In SDT-1, the FDDT in ethylene-air mixtures (without hydrogen) was registered at $\Phi > 0.6$, while, in the leaner mixtures, the FDDT was not obtained. Note that for ethylene-air mixtures, the lower detonability limit was 3.5%(vol.) C_2H_4 ($\Phi = 0.52$), as reported in [61].

Figure 15 shows an example demonstrating the extension of the concentration limits of the FDDT in SDT-2 compared to SDT-1 for a fuel containing 30%(vol.) C_2H_4 and 70%(vol.) H_2 at $\Phi = 0.50$. In the initial stages, flame acceleration in SDT-1 and SDT-2 looked almost the same up to distances of 1.7–1.8 m from the ignition source. Thereafter, the FDDT occurred in SDT-2 between the second and third coils of the helical tube section, whereas the FDDT failed in SDT-1; the flame-born shock wave exited the coils at a velocity below 1200 m/s and decayed. When Φ decreased to 0.48, the FDDT was still registered in SDT-2. At the fuel-lean concentration limit of FDDT, the minimum apparent propagation velocity of the reaction front at the inlet to the helical tube section was almost constant and close to 500 m/s. When diluting hydrogen with ethylene by 10, 20, 30, and 40%, this velocity was 450 ± 60 m/s ($\Phi^* \approx 0.40$), 470 ± 50 m/s ($\Phi^* \approx 0.44$), 450 ± 70 ($\Phi^* \approx 0.48$), and 410 ± 90 m/s ($\Phi^* \approx 0.50$), respectively.
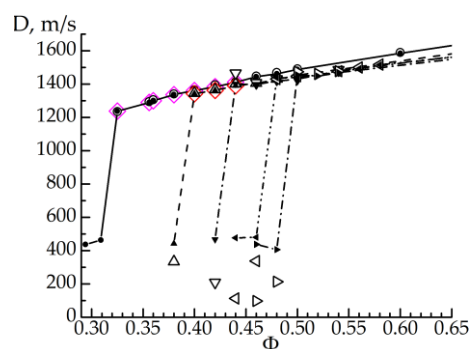
Figure 14. Dependences of the measured propagation velocities of the reaction front and the flame-born shock wave in the measuring section of SDT-2 on the fuel-to-air equivalence ratio Φ in ethylene–hydrogen–air mixtures with different dilutions of hydrogen with ethylene. Open circles correspond to the reaction front velocity D_f; filled circles correspond to the shock wave velocity D_{SW}; circles connected with a solid line correspond to 100% H_2; triangles 8 and ▲ connected with a dotted line correspond to 10% C_2H_4 + 90% H_2; triangles X and ▼ connected with a dash-dotted line correspond to 20% C_2H_4 + 80% H_2; triangles Ξ and ◄ connected with a double dash-dotted line correspond to 30% C_2H_4 + 70% H_2; triangles χ and ► connected with a double dash-dotted line correspond to 40% C_2H_4 + 60% H_2.

(**a**)

(**b**)
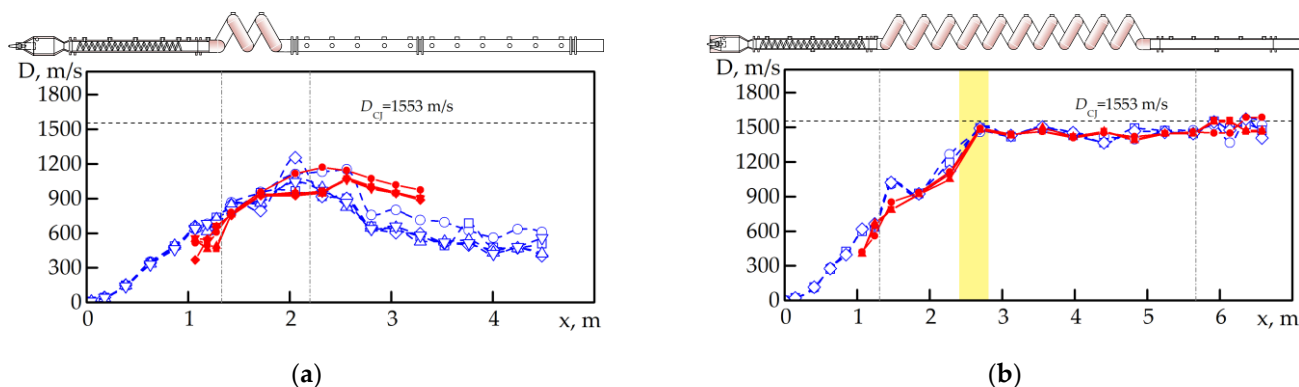
Figure 15. D–x diagrams for several shots with a fuel-lean (30% C_2H_4 + 70% H_2)–air mixture with Φ = 0.50. (**a**) SDT-1, no detonation; (**b**) SDT-2, detonation in the helical tube section and in the measuring section. The horizontal dashed lines correspond to the CJ detonation velocity; different symbols correspond to different shots; open symbols connected by a dotted line correspond to the reaction front velocity D_f; filled symbols connected by a solid line correspond to the shock wave velocity D_{SW}.

The maximum measured DDT run-up distance was attained for (20% C_2H_4 + 80% H_2)-air mixture at Φ = 0.44 (see Appendix A) with a value of 4.69 m along the facility centerline, i.e., DDT always occurred inside the helical tube of the SDT-2.

4. Conclusions

In this manuscript, we continued the study of the FDDT in tubes filled with gaseous explosive mixtures. The concept of FDDT implies the adoption of special means for flame acceleration and the amplification of the flame-born shock wave. For flame acceleration we used a Shchelkin spiral, and for shock wave amplification we used a helical tube section providing gas-dynamic focusing of the flame-born shock wave. Based on our previous studies and the results obtained in the pulsed detonation tube SDT-1, we developed a new pulsed detonation tube, SDT-2, with a longer helical tube section containing ten rather than two coils. Using SDT-2, we studied the influence of the number of coils in the helical tube section on the FDDT in air mixtures of hydrogen, methane, propane, and ethylene, as

well as binary methane-hydrogen, propane-hydrogen, and ethylene-hydrogen fuels, under normal conditions. Despite FDDT mainly occurring inside the helical tube of SDT-2, it was designed for studies of FDDT in both gaseous and heterogeneous fuel-air mixtures, which could potentially have a larger DDT run-up distance. Therefore, SDT-2 was designed with some reserve in terms of the helical tube length. Similar to SDT-1, the SDT-2 facility was used to rank the various gaseous and heterogeneous fuel-air mixtures by their detonability in terms of DDT run-up distance and time. This ranking is different from the common approach based on ranking fuel-air mixtures by their detonability in terms of the detonation cell size; the former accounts for both the low-temperature and high-temperature reactivity of fuels during flame propagation and preflame self-ignition, while the latter is relevant only to high-temperature reactivity of fuels during propagation of developed detonations.

In this study, the following new results were obtained:

(1) The possibility of a significant reduction in the detonation run-up distance in the studied fuel-air mixtures in comparison with that of the SDT-1 was demonstrated;

(2) The possibility of a significant extension of the fuel-lean concentration limit of the fast deflagration-to-detonation transition in the studied fuel-air mixtures in comparison with that of the SDT-1 was demonstrated; in sufficiently long helical tubes, fast deflagration-to-detonation transition is possible in explosive mixtures of such a composition, for which classical DDT is impossible in straight tubes with smooth or rough walls;

(3) The minimum apparent propagation velocity of the reaction front at the entrance to the helical tube section at the fuel-lean concentration limit of fast deflagration-to-detonation transition turned out to be virtually constant and close to 400–500 m/s for all studied fuel-air mixtures;

(4) For all studied fuel-air mixtures, steady-state propagation of detonation in the helical tube section with a velocity deficit above 10% was recorded, which is impossible when detonation propagates in a straight tube with smooth walls.

Author Contributions: Conceptualization, S.M.F. and I.O.S.; methodology, I.O.S.; formal analysis, I.O.S., S.M.F. and M.V.K.; investigation, I.O.S., V.S.A., M.V.K. and P.A.G.; data curation, I.O.S. and M.V.K.; writing—original draft preparation, S.M.F. and I.O.S.; writing—review and editing, S.M.F.; supervision, S.M.F.; project administration, S.M.F.; funding acquisition, S.M.F. All authors have read and agreed to the published version of the manuscript.

Data Availability Statement: The data are available on request.

Conflicts of Interest: The authors declare no conflict of interest.

Abbreviations

CJ	Chapman-Jouguet
DDT	Deflagration-to-detonation transition
FDDT	Fast deflagration-to-detonation transition
IP	Ionization probe
NPT	Normal pressure and temperature
PS	Pressure sensor
SDT-1	Standard pulsed detonation tube (version 1)
SDT-2	Standard pulsed detonation tube (version 2)

Appendix A

Table A1. Summary table of experiments conducted in SDT-2 facility with air mixtures of unitary and binary fuels. The table background is used to distinct mixtures of different compositions in terms of fuel and hydrogen content.

Gas	X_{H2}	Φ	X_{f1}	X_{f2}	X_f	$D_{f,in}$	Mode	D_{CJ}	D_{SW1}	D_{SW2}	L_{DDT}	T_{DDT}
	%		%	%	%	m/s	*)	m/s	m/s	m/s	m	ms
CH_4	0	0.7	6.83	—	6.83	152 ± 4	F	1655	374 ± 127	468 ± 23	–	–
CH_4	0	0.8	7.73	—	7.73	573 ± 76	D/F	1718	1567 ± 27	1162 ± 104	4.04	19.38
CH_4	0	0.9	8.61	—	8.61	707 ± 45	D/F	1766	1611 ± 9	1245 ± 145	2.44	14.18
CH_4	0	1	9.48	—	9.48	671 ± 18	D	1802	1644 ± 10	1720 ± 16	2.55	13.62
CH_4	10	0.7	6.61	0.73	7.34	247 ± 117	F	1659	539 ± 368	496 ± 5	–	–
CH_4	10	1	9.15	1.02	10.17	819 ± 29	D	1806	1642 ± 24	1773 ± 33	2.43	12.13
CH_4	20	0.7	6.35	1.59	7.94	346 ± 44	F	1664	840 ± 72	1067 ± 70	–	–
CH_4	20	1	8.7	2.18	10.88	909 ± 32	D	1811	1645 ± 9	1730 ± 17	2.47	10.92
CH_4	30	0.7	6.05	2.59	8.64	547 ± 34	D/F	1669	1528 ± 33	1150 ± 97	4.33	18.60
CH_4	30	1	8.34	3.57	11.91	880 ± 31	D	1818	1655 ± 4	1796 ± 45	2.48	9.89
CH_4	40	0.6	4.94	3.30	8.24	172 ± 23	F	1598	433 ± 24	489 ± 10	–	–
CH_4	40	0.7	5.69	3.79	9.48	755 ± 36	D/F	1675	1535 ± 16	1201 ± 93	2.55	13.78
CH_4	40	1	7.81	5.21	13.02	798 ± 20	D	1825	1667 ± 7	1779 ± 26	2.57	8.73
CH_4	50	0.58	4.43	4.43	8.86	308 ± 72	F	1588	664 ± 161	807 ± 34	–	–
CH_4	50	0.6	4.57	4.57	9.14	496 ± 10	D/F	1606	1461 ± 371	1546 ± 20	5.24	20.83
CH_4	50	0.62	4.71	4.71	9.42	580 ± 25	D/F	1622	1505 ± 2	1153 ± 141	3.90	17.71
CH_4	50	0.64	4.84	4.84	9.68	672 ± 29	D/F	1638	1493 ± 7	1191 ± 97	2.66	14.88
CH_4	50	0.66	4.98	4.98	9.96	798 ± 28	D	1654	1499 ± 7	1589 ± 14	2.75	13.82
CH_4	50	0.7	5.25	5.25	10.50	818 ± 28	D	1683	1544 ± 5	1635 ± 26	2.68	11.86
CH_4	50	1	7.18	7.18	14.36	769 ± 10	D	1835	1681 ± 12	1771 ± 16	2.50	7.71
CH_4	60	0.5	3.48	5.21	8.69	151 ± 80	F	1521	439 ± 94	426 ± 10	–	–
CH_4	60	0.52	3.60	5.41	9.01	172 ± 26	F	1541	429 ± 13	454 ± 4	–	–
CH_4	60	0.54	3.73	5.60	9.33	210 ± 13	F	1561	529 ± 41	508 ± 13	–	–
CH_4	60	0.56	3.86	5.78	9.64	523 ± 23	D	1580	1423 ± 113	1553 ± 24	5.25	21.30
CH_4	60	0.58	3.98	5.97	9.95	637 ± 4	D/F	1598	1464 ± 23	1252 ± 114	3.56	17.18
CH_4	60	0.6	4.10	6.16	10.26	806 ± 179	D/F	1615	1469 ± 13	1414 ± 83	2.89	14.80
CH_4	60	0.62	4.22	6.34	10.56	848 ± 56	D	1632	1488 ± 24	1554 ± 9	2.71	13.35
CH_4	60	0.64	4.34	6.52	10.86	789 ± 31	D	1648	1501 ± 20	1585 ± 10	2.77	12.44
CH_4	60	0.7	4.70	7.06	11.76	711 ± 10	D	1693	1548 ± 12	1676 ± 48	2.95	10.46
CH_4	60	0.8	5.29	7.93	13.22	725 ± 8	D	1757	1608 ± 5	1709 ± 19	2.57	8.09
CH_4	60	0.9	5.85	8.78	14.63	767 ± 58	D	1808	1668 ± 30	1762 ± 14	2.36	6.88
CH_4	60	1	6.40	9.60	16.00	767 ± 8	D	1847	1694 ± 8	1768 ± 18	2.33	6.58
CH_4	70	0.48	2.87	6.71	9.58	165 ± 51	F	1512	469 ± 8	465 ± 4	–	–
CH_4	70	0.5	2.98	6.95	9.93	423 ± 79	D	1533	903 ± 19	1546 ± 64	5.61	23.68
CH_4	70	0.54	3.19	7.45	10.64	700 ± 14	D/F	1573	1442 ± 0	1260 ± 95	2.88	15.60
CH_4	70	0.6	3.50	8.18	11.68	672 ± 9	D/F	1627	1485 ± 9	1439 ± 76	2.88	11.96
CH_4	70	0.7	4.02	9.37	13.39	714 ± 16	D	1706	1570 ± 3	1635 ± 14	2.58	8.33
CH_4	70	1	5.42	12.65	18.07	753 ± 24	D	1863	1723 ± 7	1813 ± 9	2.24	5.49
CH_4	80	0.40	1.90	7.58	9.48	85 ± 3	F	1435	455 ± 58	412 ± 9	–	–
CH_4	80	0.42	1.98	7.93	9.91	68 ± 6	F	1459	433 ± 9	434 ± 6	–	–
CH_4	80	0.44	2.07	8.26	10.33	226 ± 22	F	1483	525 ± 23	498 ± 5	–	–
CH_4	80	0.46	2.15	8.60	10.75	502 ± 28	D/F	1506	1401 ± 20	998 ± 84	4.66	21.15
CH_4	80	0.5	2.32	9.26	11.58	759 ± 75	D/F	1549	1419 ± 14	1359 ± 77	2.69	14.60
CH_4	80	0.54	2.48	9.91	12.39	689 ± 23	D/F	1589	1456 ± 9	1429 ± 68	2.99	12.14
CH_4	80	0.56	2.56	10.23	12.79	685 ± 17	D	1608	1478 ± 7	1537 ± 12	2.76	10.93
CH_4	80	0.6	2.72	10.86	13.58	658 ± 10	D	1644	1512 ± 4	1584 ± 10	2.60	9.27
CH_4	80	0.7	3.10	12.39	15.49	669 ± 5	D	1724	1592 ± 6	1669 ± 8	2.29	6.75
CH_4	80	1	4.15	16.60	20.75	763 ± 15	D	1885	1748 ± 0	1813 ± 14	2.22	4.61
CH_4	90	0.36	1.04	9.36	10.40	38 ± 1	F	1403	394 ± 10	431 ± 5	–	–
CH_4	90	0.38	1.09	9.85	10.94	202 ± 78	F	1430	489 ± 52	497 ± 7	–	–
CH_4	90	0.40	1.14	10.28	11.42	513 ± 11	D/F	1456	1329 ± 7	960 ± 82	3.93	21.40
CH_4	90	0.42	1.19	10.73	11.92	714 ± 23	D/F	1481	1348 ± 6	1025 ± 82	2.94	17.31

Table A1. *Cont.*

Gas	X_{H2}	Φ	X_{f1}	X_{f2}	X_f	$D_{f,in}$	Mode	D_{CJ}	D_{SW1}	D_{SW2}	L_{DDT}	T_{DDT}
CH$_4$	90	0.44	1.24	11.18	12.42	720 ± 14	D/F	1505	1372 ± 16	1055 ± 78	2.88	15.17
CH$_4$	90	0.46	1.29	11.61	12.90	638 ± 16	D/F	1528	1403 ± 0	1277 ± 71	3.06	13.79
CH$_4$	90	0.48	1.34	12.06	13.40	635 ± 5	D/F	1550	1421 ± 3	1400 ± 47	3.01	12.39
CH$_4$	90	0.5	1.39	12.49	13.88	657 ± 16	D	1572	1439 ± 7	1501 ± 4	2.93	11.16
CH$_4$	90	0.7	1.84	16.57	18.41	731 ± 27	D	1750	1622 ± 3	1664 ± 25	2.24	5.51
CH$_4$	90	1	2.44	21.93	24.37	1407 ± 131	D	1917	1791 ± 5	1855 ± 18	1.33	3.08
C$_2$H$_4$	0	0.7	4.66	—	4.66	775 ± 48	D	1692	1570 ± 9	1664 ± 9	2.24	12.97
C$_2$H$_4$	0	1	6.53	—	6.53	1407 ± 194	D	1822	1703 ± 3	1824 ± 5	1.32	6.01
C$_2$H$_4$	10	0.7	4.55	0.51	5.06	791 ± 36	D	1694	1566 ± 13	1662 ± 8	2.38	12.49
C$_2$H$_4$	10	1	6.37	0.71	7.08	1464 ± 29	D	1825	1706 ± 8	1825 ± 8	1.32	5.74
C$_2$H$_4$	20	0.7	1.43	1.11	5.54	737 ± 22	D	1696	1572 ± 5	1679 ± 5	2.28	11.47
C$_2$H$_4$	20	1	6.18	1.55	7.73	1305 ± 163	D	1828	1705 ± 0	1813 ± 1	1.35	5.57
C$_2$H$_4$	30	0.7	4.28	1.84	6.12	740 ± 21	D	1699	1570 ± 1	1666 ± 3	2.39	10.86
C$_2$H$_4$	30	1	5.96	2.56	8.52	1350 ± 75	D	1831	1710 ± 3	1817 ± 5	1.34	5.29
C$_2$H$_4$	40	0.7	4.1	2.73	6.83	724 ± 9	D	1702	1572 ± 12	1664 ± 8	2.28	10.12
C$_2$H$_4$	40	1	5.69	3.79	9.48	1188 ± 290	D	1836	1714 ± 6	1836 ± 6	1.37	5.10
C$_2$H$_4$	50	0.5	2.82	2.82	5.65	218 ± 11	F	1542	521 ± 45	489 ± 5	–	–
C$_2$H$_4$	50	0.7	3.86	3.86	7.73	708 ± 25	D	1706	1581 ± 5	1684 ± 7	2.25	9.26
C$_2$H$_4$	50	1	5.34	5.34	10.7	1276 ± 85	D	1842	1721 ± 5	1837 ± 5	1.35	4.74
C$_2$H$_4$	60	0.46	2.41	3.62	6.04	122 ± 33	F	1519	437 ± 85	452 ± 17	–	–
C$_2$H$_4$	60	0.48	2.51	3.77	6.28	196 ± 55	F	1526	406 ± 32	456 ± 27	–	–
C$_2$H$_4$	60	0.5	2.61	3.92	6.53	408 ± 88	D	1547	1454 ± 33	1580 ± 41	4.26	25.82
C$_2$H$_4$	60	0.52	2.70	4.06	6.76	570 ± 9	D	1567	1448 ± 4	1489 ± 13	2.72	20.38
C$_2$H$_4$	60	0.54	2.81	4.21	7.02	744 ± 28	D	1586	1469 ± 5	1513 ± 10	2.47	16.92
C$_2$H$_4$	60	0.7	3.56	5.34	8.90	707 ± 37	D	1712	1585 ± 6	1694 ± 3	2.24	8.36
C$_2$H$_4$	60	1	4.90	7.35	12.25	1168 ± 189	D	1850	1732 ± 2	1843 ± 15	1.37	4.42
C$_2$H$_4$	70	0.44	2.06	4.81	6.87	126 ± 9	F	1488	476 ± 20	507 ± 24	–	–
C$_2$H$_4$	70	0.46	2.15	5.01	7.16	243 ± 42	F	1511	480 ± 32	490 ± 6	–	–
C$_2$H$_4$	70	0.48	2.23	5.21	7.44	453 ± 73	D	1556	1437 ± 17	1496 ± 15	4.53	24.14
C$_2$H$_4$	70	0.5	2.32	5.40	7.72	647 ± 15	D	1553	1439 ± 7	1505 ± 35	2.61	18.58
C$_2$H$_4$	70	0.54	2.49	5.81	8.30	736 ± 20	D	1592	1471 ± 10	1585 ± 46	2.58	14.51
C$_2$H$_4$	70	0.56	2.57	6.01	8.58	737 ± 56	D	1610	1493 ± 6	1585 ± 19	2.60	13.00
C$_2$H$_4$	70	0.58	2.66	6.20	8.85	744 ± 42	D	1628	1516 ± 7	1630 ± 13	2.58	11.49
C$_2$H$_4$	70	0.7	3.15	7.34	10.49	767 ± 49	D	1720	1593 ± 4	1654 ± 20	2.24	7.54
C$_2$H$_4$	70	1	4.30	10.03	14.33	1406 ± 129	D	1862	1742 ± 3	1846 ± 7	1.33	4.02
C$_2$H$_4$	70	1.4	5.70	13.30	19.00	1445 ± 108	D	1935	1803 ± 8	1905 ± 6	1.33	4.85
C$_2$H$_4$	80	0.42	1.62	6.47	8.09	125 ± 5	F	1473	466 ± 23	445 ± 7	–	–
C$_2$H$_4$	80	0.44	1.69	6.75	8.44	467 ± 48	D	1497	1399 ± 37	1447 ± 18	4.69	24.10
C$_2$H$_4$	80	0.46	1.76	7.03	8.79	569 ± 21	D	1519	1398 ± 2	1485 ± 23	3.12	20.15
C$_2$H$_4$	80	0.48	1.83	7.30	9.13	775 ± 24	D	1541	1418 ± 8	1435 ± 22	2.53	16.36
C$_2$H$_4$	80	0.5	1.90	7.58	9.48	748 ± 51	D	1562	1429 ± 65	1533 ± 30	2.58	14.75
C$_2$H$_4$	80	0.54	2.03	8.14	10.17	690 ± 49	D	1601	1479 ± 6	1630 ± 46	2.61	11.94
C$_2$H$_4$	80	0.7	2.56	10.22	12.78	698 ± 11	D	1731	1601 ± 9	1674 ± 13	2.24	6.68
C$_2$H$_4$	80	1	3.46	13.86	17.32	1483 ± 34	D	1879	1759 ± 4	1839 ± 13	1.32	3.55
C$_2$H$_4$	90	0.38	0.96	8.63	9.59	166 ± 50	F	1436	441 ± 5	457 ± 21	–	–
C$_2$H$_4$	90	0.4	1.00	9.04	10.05	446 ± 62	D/F	1462	1342 ± 6	976 ± 44	3.82	22.71
C$_2$H$_4$	90	0.42	1.05	9.45	10.50	664 ± 28	D/F	1487	1362 ± 4	1062 ± 40	2.77	18.18
C$_2$H$_4$	90	0.44	1.09	9.85	10.94	693 ± 21	D/F	1497	1389 ± 2	1477 ± 35	2.64	15.65
C$_2$H$_4$	90	0.46	1.14	10.26	11.40	660 ± 34	D	1519	1403 ± 0	1454 ± 15	2.97	14.44
C$_2$H$_4$	90	0.48	1.19	10.73	11.92	643 ± 33	D	1556	1428 ± 7	1541 ± 41	2.81	12.14
C$_2$H$_4$	90	0.5	1.22	11.02	12.24	652 ± 10	D	1577	1453 ± 0	1518 ± 21	2.66	11.28
C$_2$H$_4$	90	0.7	1.64	14.73	16.37	780 ± 71	D	1751	1624 ± 9	1768 ± 26	2.23	5.46
C$_2$H$_4$	90	1	2.18	19.65	21.83	1513 ± 88	D	1908	1774 ± 6	1892 ± 4	0.62	2.63
C$_3$H$_8$	0	0.7	2.85	—	2.85	285 ± 92	F	1660	624 ± 74	625 ± 60	–	–
C$_3$H$_8$	0	0.71	2.89	—	2.89	383 ± 80	F+D	1667	917 ± 0	1669 ± 69	5.80	44.93
C$_3$H$_8$	0	0.72	2.93	—	2.93	352 ± 78	D	1673	1635 ± 40	1633 ± 17	5.14	44.31
C$_3$H$_8$	0	0.74	3.01	—	3.01	528 ± 37	D	1686	1561 ± 13	1669 ± 20	3.32	31.43
C$_3$H$_8$	0	0.76	3.09	—	3.09	560 ± 27	D	1697	1571 ± 5	1684 ± 20	2.58	25.52
C$_3$H$_8$	0	0.8	3.24	—	3.24	690 ± 17	D	1719	1591 ± 4	1674 ± 15	2.31	20.76

Table A1. *Cont.*

Gas	X_{H2}	Φ	X_{f1}	X_{f2}	X_f	$D_{f,in}$	Mode	D_{CJ}	D_{SW1}	D_{SW2}	L_{DDT}	T_{DDT}
C_3H_8	0	1	4.02	—	4.02	874 ± 25	D	1798	1660 ± 0	1773 ± 12	2.22	11.75
C_3H_8	10	0.7	2.81	0.31	3.12	336 ± 46	D	1662	1430 ± 184	1638 ± 17	4.62	39.42
C_3H_8	10	1	3.96	0.44	4.40	830 ± 33	D	1800	1664 ± 3	1779 ± 6	2.22	11.30
C_3H_8	20	0.7	2.76	0.69	3.45	447 ± 52	D	1663	1540 ± 11	1676 ± 46	3.98	33.67
C_3H_8	20	1	3.89	0.97	4.86	817 ± 28	D	1802	1667 ± 4	1786 ± 9	2.23	10.80
C_3H_8	30	0.7	2.7	1.16	3.86	543 ± 76	D	1665	1537 ± 10	1676 ± 21	3.34	26.95
C_3H_8	30	1	3.8	1.63	5.43	800 ± 21	D	1805	1668 ± 6	1779 ± 7	2.24	10.15
C_3H_8	40	0.7	2.63	1.75	4.38	523 ± 19	D	1668	1545 ± 13	1694 ± 38	2.58	22.51
C_3H_8	40	1	3.69	2.46	6.15	774 ± 10	D	1809	1670 ± 0	1802 ± 11	2.24	9.60
C_3H_8	50	0.7	2.53	2.53	5.06	669 ± 30	D	1672	1547 ± 4	1674 ± 35	2.53	19.34
C_3H_8	50	1	3.54	3.54	7.08	772 ± 10	D	1814	1678 ± 6	1825 ± 20	2.22	8.82
C_3H_8	60	0.5	1.74	2.62	4.36	–	X	1510	–	–	–	–
C_3H_8	60	0.58	2.01	3.01	5.02	219 ± 43	F	1585	443 ± 68	479 ± 8	–	–
C_3H_8	60	0.6	2.07	3.11	5.18	293 ± 62	F	1602	624 ± 192	821 ± 56	–	–
C_3H_8	60	0.62	2.14	3.21	5.35	475 ± 56	D	1618	1429 ± 7	1563 ± 10	4.13	27.47
C_3H_8	60	0.7	2.40	3.60	6.00	814 ± 14	D	1677	1554 ± 0	1735 ± 54	2.22	15.88
C_3H_8	60	1	3.34	5.01	8.35	773 ± 21	D	1820	1687 ± 3	1825 ± 17	2.22	8.07
C_3H_8	70	0.5	1.61	3.75	5.36	42 ± 5	F	1517	356 ± 10	356 ± 2	–	–
C_3H_8	70	0.6	1.91	4.45	6.36	563 ± 8	D	1609	1445 ± 75	1550 ± 19	3.94	23.25
C_3H_8	70	0.7	2.20	5.14	7.34	766 ± 10	D	1685	1543 ± 4	1709 ± 49	2.56	14.03
C_3H_8	70	1	3.05	7.12	10.17	773 ± 30	D	1830	1698 ± 4	1819 ± 6	2.23	7.16
C_3H_8	80	0.5	1.39	5.57	6.96	134 ± 36	F	1528	408 ± 13	455 ± 10	–	–
C_3H_8	80	0.52	1.44	5.78	7.22	200 ± 25	F	1548	505 ± 38	498 ± 6	–	–
C_3H_8	80	0.53	1.47	5.88	7.35	402 ± 47	D	1558	1461 ± 27	1517 ± 12	4.71	25.96
C_3H_8	80	0.54	1.50	5.98	7.48	465 ± 63	D	1567	1480 ± 15	1559 ± 30	4.73	24.46
C_3H_8	80	0.6	1.65	6.59	8.24	805 ± 41	D	1621	1500 ± 6	1576 ± 10	2.28	15.10
C_3H_8	80	0.7	1.90	7.58	9.48	721 ± 10	D	1698	1568 ± 3	1635 ± 12	2.57	10.49
C_3H_8	80	1	2.60	10.42	13.02	763 ± 34	D	1846	1718 ± 0	1813 ± 25	2.23	6.11
C_3H_8	90	0.42	0.85	7.63	8.48	106 ± 10	F	1460	399 ± 24	432 ± 3	–	–
C_3H_8	90	0.44	0.88	7.96	8.84	143 ± 32	F	1484	435 ± 24	465 ± 10	–	–
C_3H_8	90	0.46	0.92	8.29	9.21	513 ± 28	D/F	1506	1409 ± 39	1072 ± 85	4.20	23.34
C_3H_8	90	0.48	0.96	8.61	9.57	622 ± 12	D	1528	1404 ± 4	1466 ± 10	2.86	18.83
C_3H_8	90	0.5	0.99	8.94	9.93	743 ± 24	D	1549	1430 ± 8	1529 ± 30	2.53	16.02
C_3H_8	90	0.6	1.16	10.52	11.68	700 ± 28	D	1644	1520 ± 4	1616 ± 14	2.58	10.18
C_3H_8	90	0.7	1.34	12.03	13.37	708 ± 34	D	1722	1598 ± 9	1704 ± 9	2.26	7.22
C_3H_8	90	1	1.81	16.26	18.07	1061 ± 88	D	1878	1749 ± 11	1813 ± 15	1.50	4.19
—	100	0.295	—	11	11	– **)	F	1337	437 ± 17	425 ± 7	–	–
—	100	0.310	—	11.5	11.5	– **)	F	1362	463 ± 6	447 ± 6	–	–
—	100	0.326	—	12	12	339 ± 94	D/F	1385	1237 ± 35	964 ± 53	3.97	24.66
—	100	0.357	—	13	13	740 ± 88	D/F	1431	1289 ± 19	977 ± 69	3.06	18.29
—	100	0.36	—	13.11	13.11	642 ± 33	D/F	1434	1300 ± 12	982 ± 70	3.04	17.63
—	100	0.38	—	13.73	13.73	583 ± 9	D/F	1462	1336 ± 18	1008 ± 97	3.14	15.39
—	100	0.4	—	14.35	14.35	509 ± 16	D/F	1488	1361 ± 6	1114 ± 60	3.11	13.74
—	100	0.42	—	14.96	14.96	548 ± 32	D/F	1514	1383 ± 10	1434 ± 26	3.04	12.03
—	100	0.44	—	15.57	15.57	505 ± 95	D/F	1539	1411 ± 7	1448 ± 68	3.01	10.89
—	100	0.46	—	16.16	16.16	548 ± 50	D	1562	1444 ± 10	1521 ± 20	2.68	9.39
—	100	0.48	—	16.74	16.74	572 ± 35	D	1585	1461 ± 5	1531 ± 9	2.61	8.68
—	100	0.5	—	17.32	17.32	632 ± 40	D	1607	1487 ± 21	1551 ± 17	2.56	7.87
—	100	0.6	—	20.09	20.09	1194 ± 40	D	1707	1585 ± 32	1690 ± 27	1.60	4.83
—	100	0.7	—	22.68	22.68	1349 ± 51	D	1791	1677 ± 18	1772 ± 39	1.34	3.64
—	100	1	—	29.57	29.57	1759 ± 36	D	1967	1858 ± 13	1960 ± 23	0.62	2.05

*) Propagation mode of the reaction wave: X—no ignition, F—flame, D—detonation, D/F—detonation in the helical tube section and detonation decay in the measuring section, F + D—flame in some shots and detonation in other shots (limiting mode), X_{f1}—volume fraction of fuel 1 in the fuel-air mixture, X_{f2}—volume fraction of fuel 2 in the fuel-air mixture, X_f—volume fraction of fuel in the fuel-air mixture ($X_f = X_{f1} + X_{f2}$), X_{H2}—volume fraction of hydrogen in the binary fuel ($C_nH_m + H_2$), $D_{f,in}$—the apparent propagation velocity of the reaction front at the entrance to the helical tube section with the root-mean-square deviation in three shots, D_{CJ}—CJ detonation velocity, D_{SW1}—steady-state detonation velocity in the helical tube section, D_{SW2}—steady-state detonation velocity in the measuring section, L_{DDT}—FDDT run-up distance (mean value over three shots), T_{DDT}—FDDT run-up time (mean value over three shots). **) Flame propagates with acoustic effect; however, flame is not registered by IPs.

References

1. Bone, W.A.; Fraser, R.P. A photographic investigation of flame movements in carbonic oxide-oxygen explosions. *Philos. Trans. R. Soc. London. Ser. A Contain. Pap. A Math. Or Phys. Character* **1929**, *228*, 197–234. [CrossRef]
2. Zel'dovich, Y.B. *The Theory of Combustion and Detonation of Gases*; Academy of Sciences of the Soviet Union: Moscow, Russia, 1944.
3. Oppenheim, A.K. *Introduction to Gasdynamics of Explosions*; Springer: New York, NY, USA, 1972.
4. Shchelkin, K.I. *Fast Combustion and Spinning Detonation of Gases*; Voenizdat: Moscow, Russia, 1949.
5. Lindstedt, R.P.; Michels, H.J. Deflagration to detonation transitions and strong deflagrations in alkane and alkene air mixtures. *Combust. Flame* **1989**, *76*, 169–181. [CrossRef]
6. Sorin, R.; Zitoun, R.; Desbordes, D. Optimization of the deflagration to detonation transition: Reduction of length and time of transition. *Shock Waves* **2006**, *15*, 137–145. [CrossRef]
7. Theodorczyk, A.; Lee, J.H.S.; Knystautas, R. Propagation Mechanism of Quasidetonations. *Symp. Int. Combustion* **1988**, *22*, 1723–1731. [CrossRef]
8. Lee, J.H.S. *The Detonation Phenomenon*; The Cambridge University Press: New York, NY, USA, 2008.
9. Feng, X.; Huang, X. Influence of variable blocking ratio on DDT process. *Energies* **2022**, *15*, 7706. [CrossRef]
10. Frolov, S.M. Initiation of strong reactive shocks and detonation by traveling ignition pulses. *J. Loss Prev. Process Ind.* **2006**, *19*, 238–244. [CrossRef]
11. Frolov, S.M. Fast deflagration-to-detonation transition. *Russ. J. Phys. Chem. B* **2008**, *2*, 442–455. [CrossRef]
12. Frolov, S.M.; Semenov, I.V.; Komissarov, P.V.; Utkin, P.S.; Markov, V.V. Reduction of the deflagration-to-detonation transition distance and time in a tube with regular shaped obstacles. *Doklady Phys. Chem.* **2007**, *415*, 209–213. [CrossRef]
13. Li, J.-M.; Teo, C.J.; Lim, K.S.; Wen, C.-S.; Khoo, B.C. Deflagration to detonation transition by hybrid obstacles in pulse detonation engines. In Proceedings of the 49th AIAA/ASME/SAE/ASEE Joint Propulsion Conference, San Jose, CA, USA, 14–17 July 2013; pp. 2013–3657. [CrossRef]
14. Coates, A.M.; Mathias, D.L.; Cantwell, B.J. Numerical investigation of the effect of obstacle shape on deflagration to detonation transition in a hydrogen–air mixture. *Combust. Flame* **2019**, *209*, 278–290. [CrossRef]
15. Xiao, H.; Oran, E.S. Flame acceleration and deflagration-to-detonation transition in hydrogen-air mixture in a channel with an array of obstacles of different shapes. *Combust. Flame* **2020**, *220*, 378–393. [CrossRef]
16. Liu, Z.; Li, X.; Li, M.; Xiao, H. Flame acceleration and DDT in a channel with fence-type obstacles: Effect of obstacle shape and arrangement. *Proc. Combust. Inst.* **2022**, in press. [CrossRef]
17. Li, T.; Wang, X.; Xu, B.; Kong, F. An efficient approach to achieve flame acceleration and transition to detonation. *Phys. Fluids* **2021**, *33*, 056103. [CrossRef]
18. Frolov, S.M.; Smetanyuk, V.A.; Aksenov, V.S.; Koval', A.S. Deflagration-to-detonation transition in crossed-flow fast jets of propellant components. *Doklady Phys. Chem.* **2017**, *476*, 153–156. [CrossRef]
19. Wang, Y.; Fan, W.; Li, S.; Zhang, Q.; Li, H. Numerical simulations of flame propagation and DDT in obstructed detonation tubes filled with fluidic obstacles. In Proceedings of the 21st AIAA International Space Planes and Hypersonics Technologies Conference, Xiamen, China, 6–9 March 2017; pp. 2017–2382.
20. Peng, H.; Huang, Y.; Deiterding, R.; You, Y.; Luan, Z. Effects of transverse jet parameters on flame propagation and detonation transition in hydrogen–oxygen–argon mixture. *Combust. Sci. Technol.* **2019**, *193*, 1516–1537. [CrossRef]
21. Starikovskaia, S. Plasma assisted ignition and combustion. *J. Phys. D Appl. Phys.* **2006**, *39*, R265–R299. [CrossRef]
22. Zhukov, V.; Starikovskii, A. Effect of a nanosecond gas discharge on deflagration to detonation transition. *Combust. Explos. Shock Waves* **2006**, *42*, 195–204. [CrossRef]
23. Gray, J.A.T.; Lacoste, D.A. Enhancement of the transition to detonation of a turbulent hydrogen–air flame by nanosecond repetitively pulsed plasma discharges. *Combust. Flame* **2019**, *199*, 258–266. [CrossRef]
24. Ciccarelli, G.; de Witt, B. Detonation initiation by shock reflection from an orifice plate. *Shock Waves* **2006**, *15*, 259–265. [CrossRef]
25. Frolov, S.M.; Aksenov, V.S. Initiation of gas detonation in a tube with a shaped obstacle. *Doklady Phys. Chem.* **2009**, *427*, 129–132. [CrossRef]
26. Habicht, F.E.; Yücel, F.C.; Gray, J.A.; Paschereit, C.O. Detonation initiation by shock focusing at elevated pressure conditions in a pulse detonation combustor. *Intern. J. Spray Combust. Dynamics* **2020**, *12*, 175682772092171. [CrossRef]
27. Frolov, S.M.; Shamshin, I.O.; Medvedev, S.N.; Dubrovskii, A.V. Initiation of detonation in a tube with a profiled central body. *Dokl. Phys. Chem.* **2011**, *438*, 114–117. [CrossRef]
28. Frolov, S.M.; Aksenov, V.S.; Shamshin, I.O. Initiation of gaseous detonation in tubes with sharp U-bends. *Dokl. Phys. Chem.* **2007**, *417*, 22–25. [CrossRef]
29. Frolov, S.M.; Aksenov, V.S.; Shamshin, I.O. Shock wave and detonation propagation through U-bend tubes. *Proc. Combust. Inst.* **2007**, *31*, 2421–2428. [CrossRef]
30. Frolov, S.M.; Aksenov, V.S.; Shamshin, I.O. Propagation of shock and detonation waves in channels with U-shaped bends of limiting curvature. *Russ. J. Phys. Chem. B* **2008**, *2*, 759–774. [CrossRef]
31. Gwak, M.-C.; Yoh, J.J. Effect of multi-bend geometry on deflagration to detonation transition of a hydrocarbon-air mixture in tubes. *Int. J. Hydrogen Energy* **2013**, *38*, 11446–11457. [CrossRef]
32. Zheng, H.; Zhu, W.; Jia, X.; Zhao, N. Eulerian–Lagrangian modeling of deflagration to detonation transition in n-decane/oxygen/nitrogen mixtures. *Phys. Fluids* **2022**, *34*, 126110. [CrossRef]

33. Pan, Z.; Zhang, Z.; Yang, H.; Gui, M.; Zhang, P.; Zhu, Y. Experimental and numerical investigation on flame propagation and transition to detonation in curved channel. *Aerospace Sci. Technol.* **2021**, *118*, 107036. [CrossRef]

34. Gai, J.; Qiu, H.; Xiong, C.; Huang, Z. Experimental investigation on the propagation process of combustion wave in the annular channel filled with acetylene-air/oxygen mixture. *Flow Turbul. Combust.* **2022**, *108*, 797–817. [CrossRef]

35. Frolov, S.M.; Basevich, V.Y.; Aksenov, V.S.; Polikhov, S.A. Optimization study of spray detonation initiation by electric discharge. *Shock Waves* **2005**, *14*, 175–186. [CrossRef]

36. Frolov, S.M.; Aksenov, V.S.; Basevich, V.Y. Initiation of heterogeneous detonation in tubes with coils and Shchelkin spiral. *High Temp.* **2006**, *44*, 283–290. [CrossRef]

37. Frolov, S.M.; Aksenov, V.S. Deflagration-to-detonation transition in a kerosene–air mixture. *Doklady Phys. Chem.* **2007**, *416*, 261–264. [CrossRef]

38. Frolov, S.M.; Semenov, I.V.; Ahmedyanov, I.F.; Markov, V.V. Shock-to-Detonation Transition in Tube Coils. In *Shock Waves: 26th International Symposium on Shock Waves*; Hannemann, K., Seiler, F., Eds.; Springer: Berlin/Heidelberg, Germany, 2009; Volume 1, pp. 365–370, ISBN 978-3-540-85167-7.

39. Frolov, S.M.; Basevich, V.Y.; Aksenov, V.S.; Polikhov, S.A. Detonation initiation by controlled triggering of electric discharges. *J. Propuls. Power* **2003**, *19*, 573–580. [CrossRef]

40. Frolov, S.M.; Basevich, V.Y.; Aksenov, V.S.; Polikhov, S.A. Spray detonation initiation by controlled triggering of electric discharges. *J. Propuls. Power* **2005**, *21*, 54–64. [CrossRef]

41. Frolov, S.M.; Basevich, V.Y.; Aksenov, V.S.; Polikhov, S.A. Initiation of gaseous detonation by a traveling forced ignition pulse. Doklady Phys. *Chem.* **2004**, *394*, 16–18.

42. Frolov, S.M.; Basevich, V.Y.; Aksenov, V.S.; Polikhov, S.A. Initiation of gas detonation by a travelling ignition source. *Russ. J. Chem. Phys.* **2004**, *23*, 61–67.

43. Ciccarelli, G.; Johansen, C.; Hickey, M. Flame acceleration enhancement by distributed ignition points. *J. Propuls. Power* **2005**, *21*, 1029–1034. [CrossRef]

44. Frolov, S.M.; Aksenov, V.S.; Basevich, V.Y. Detonation initiation by shock wave interaction with the prechamber jet ignition zone. *Doklady Phys. Chem.* **2006**, *410*, 255–259. [CrossRef]

45. Frolov, S.M.; Aksenov, V.S.; Basevich, V.Y. Shock-to-Detonation Transition Due to Shock Interaction with Prechamber-Jet Cloud. In *Shock Waves: 26th Intern Symp. on Shock Waves*; Hannemann, K., Seiler, F., Eds.; Springer: Berlin/Heidelberg, Germany, 2009; Volume 1, pp. 359–364, ISBN 978-3-540-85167-7.

46. Frolov, S.M.; Zvegintsev, V.I.; Aksenov, V.S.; Bilera, I.V.; Kazachenko, M.V.; Shamshin, I.O.; Gusev, P.A.; Belotserkovskaya, M.S.; Koverzanova, E.V. Detonability of air mixtures of the polypropylene pyrolysis products. *Combust. Explos.* **2018**, *11*, 44–60. [CrossRef]

47. Frolov, S.M.; Shamshin, I.O.; Aksenov, V.S.; Kazachenko, M.V.; Gusev, P.A. Ranking of gaseous fuel–air mixtures according to their detonability using a standard pulsed detonation tube. *Combust. Explos.* **2019**, *12*, 78–90. [CrossRef]

48. Frolov, S.M.; Zvegintsev, V.I.; Shamshin, I.O.; Kazachenko, M.V.; Aksenov, V.S.; Bilera, I.V.; Semenov, I.V. Detonability of air mixtures of polyethylene pyrolysis products. *Combust. Explos.* **2020**, *13*, 48–61. [CrossRef]

49. Frolov, S.M.; Zvegintsev, V.I.; Aksenov, V.S.; Bilera, I.V.; Kazachenko, M.V.; Shamshin, I.O.; Gusev, P.A.; Belotserkovskaya, M.S. Detonability of fuel–air mixtures. *Shock Waves* **2020**, *30*, 721–739. [CrossRef]

50. Frolov, S.M.; Shamshin, I.O.; Kazachenko, M.V.; Aksenov, V.S.; Bilera, I.V.; Ivanov, V.S.; Zvegintsev, V.I. Polyethylene pyrolysis products: Their detonability in air and applicability to solid-fuel detonation ramjets. *Energies* **2021**, *14*, 820. [CrossRef]

51. Shamshin, I.O.; Kazachenko, M.V.; Frolov, S.M.; Basevich, V.Y. Deflagration-to-detonation transition in air mixtures of hydrogen–methane fuel. *Combust. Explos.* **2020**, *13*, 60–75. [CrossRef]

52. Shamshin, I.O.; Kazachenko, M.V.; Frolov, S.M.; Basevich, V.Y. Deflagration-to-detonation transition in stochiometric mixtures of the binary methane–hydrogen fuel with air. *Int. J. Hydrog. Energy* **2021**, *46*, 34046–34058. [CrossRef]

53. Shamshin, I.O.; Kazachenko, M.V.; Frolov, S.M.; Basevich, V.Y. Deflagration-to-detonation transition in air mixtures of propane–hydrogen fuel. *Combust. Explos.* **2021**, *14*, 8–25. [CrossRef]

54. Shamshin, I.O.; Kazachenko, M.V.; Frolov, S.M.; Basevich, V.Y. Deflagration-to-detonation transition in stochiometric propane–hydrogen–air mixtures. *Fuels* **2022**, *3*, 667–681. [CrossRef]

55. Shamshin, I.O.; Kazachenko, M.V.; Frolov, S.M.; Basevich, V.Y. Deflagration-to-detonation transition in air mixtures of ethylene–hydrogen fuel. *Combust. Explos.* **2021**, *14*, 26–39. [CrossRef]

56. Shamshin, I.O.; Kazachenko, M.V.; Frolov, S.M.; Basevich, V.Y. Transition of deflagration to detonation in ethylene-hydrogen-air mixtures. *Int. J. Hydrogen Energy* **2022**, *47*, 16676–16685. [CrossRef]

57. Zhang, B. The influence of wall roughness on detonation limits in hydrogen–oxygen mixture. *Combust. Flame* **2016**, *169*, 333–339. [CrossRef]

58. Zhang, B.; Liu, H. The effects of large scale perturbation-generating obstacles on the propagation of detonation filled with methane–oxygen mixture. *Combust. Flame* **2017**, *182*, 279–287. [CrossRef]

59. Frolov, S.M.; Shamshin, I.O.; Aksenov, V.S.; Ivanov, V.S.; Vlasov, P.A. Ion sensors for pulsed and continuous detonation combustors. *Chemosensors* **2023**, *11*, 33. [CrossRef]

60. Borisov, A.A.; Loban', S.A. Detonation limits of hydrocarbon-air mixtures in tubes. *Combust. Explos. Shock Waves* **1977**, *13*, 618–621. [CrossRef]

61. Borisov, A.A.; Gel'fand, B.E.; Loban', S.A.; Mailkov, A.E.; Khomik, S.V. Detonation limits of fuel–air mixtures in smooth and rough tubes. *Khim. Fiz.* **1982**, *2*, 848–853.
62. Nettleton, M.A. *Gaseous Detonations: Their Nature, Effects and Control*; Chapman and Hall: London, UK, 1987.